TR / IN / 92

Solar Physics Research Corporation
Final Report: NASW-97029
1 August 1999

Project 1 PI: Charles Lindsey

Project 2 PI: Karen L. Harvey

1. HELIOSEISMIC HOLOGRAPHY: C. Lindsey and D. Braun

1.1 *SCIENTIFIC BACKGROUND*

1.1.1 Introduction

Over the period of this grant, helioseismic holography has opened a major new diagnostic avenue in local helioseismology. Applied to the SOHO-MDI Doppler observations, it has given us the discoveries of "acoustic moats" surrounding sunspots, "acoustic glories" surrounding some active regions and active-region complexes and resolved some long-standing puzzles raised by other diagnostics. Seismic holography at the higher acoustic frequencies shows "acoustic condensations" that appear to represent seismic perturbations up to 20 Mm beneath active-region photospheres. Phase-sensitive seismic holography is now giving us high-resolution refractive maps of acoustic phaseshifts caused by magnetic forces in the near solar subsurface, thermal perturbations in acoustic moats, and Doppler scattering by subsurface flows. And, comparisons between high-frequency emission from the quiet Sun and acoustic glories show a statistical anomaly that is most interesting and may give us insight into how the near solar subphotosphere produces seismic waves. Seismic holography has now given us the first acoustic images of a solar flare. Indeed, seismic holography applied to the SOHO-MDI observations is now allowing us quite literally to look into the near subphotospheres of active regions and the quiet Sun from a local perspective. What this is showing us is remarkable, and promises us a new insight into the hydromechanical and thermal environments of the near solar interior. Because of this, we think that this project should be regarded as an extraordinary success. We will begin this report with a brief synopsis of the conceptual foundation of helioseismic holography, followed by a review of developments that have come out of its development in this grant.

1.1.2 Computational Holography

Seismic holography consists in the computational reconstruction of the acoustic field at the solar surface regressively into the solar interior to render seismic images of subsurface sources that give rise to the signature seen at the surface. This has been described at length by Lindsey & Braun 1990, Braun et al. 1992, Lindsey et al. 1996, and Lindsey & Braun 1997. On the practical level, one can think of holography as a procedure which

applies observations at the surface of a wave-propagating medium to a quiet model of the medium *in time reverse*. Computationally, the task is to propagate the acoustic disturbances resulting from such a time-reverse application backwards into the interior of the model in such a way as will render an acoustic image of any localized source or sources, for example, from which the waves viewed at the surface could have emanated. Such an acoustic model, if sampled at the depth of an actual localized source will render it by a compact, positive image. An acoustic sink in the focal plane against a background of ambient acoustic noise will likewise be rendered sharply in silhouette. If the "focal plane" on which the acoustic model is sampled is moved sufficiently above or below the depth of the source or sink, the image will simply defocus, as illustrated by Figure 1. This dependence of the image focus on the submergence of the focal plane lends a powerful depth diagnostic that is quite familiar to anyone who is experienced in the practice of optical microscopy or standard optical holography.

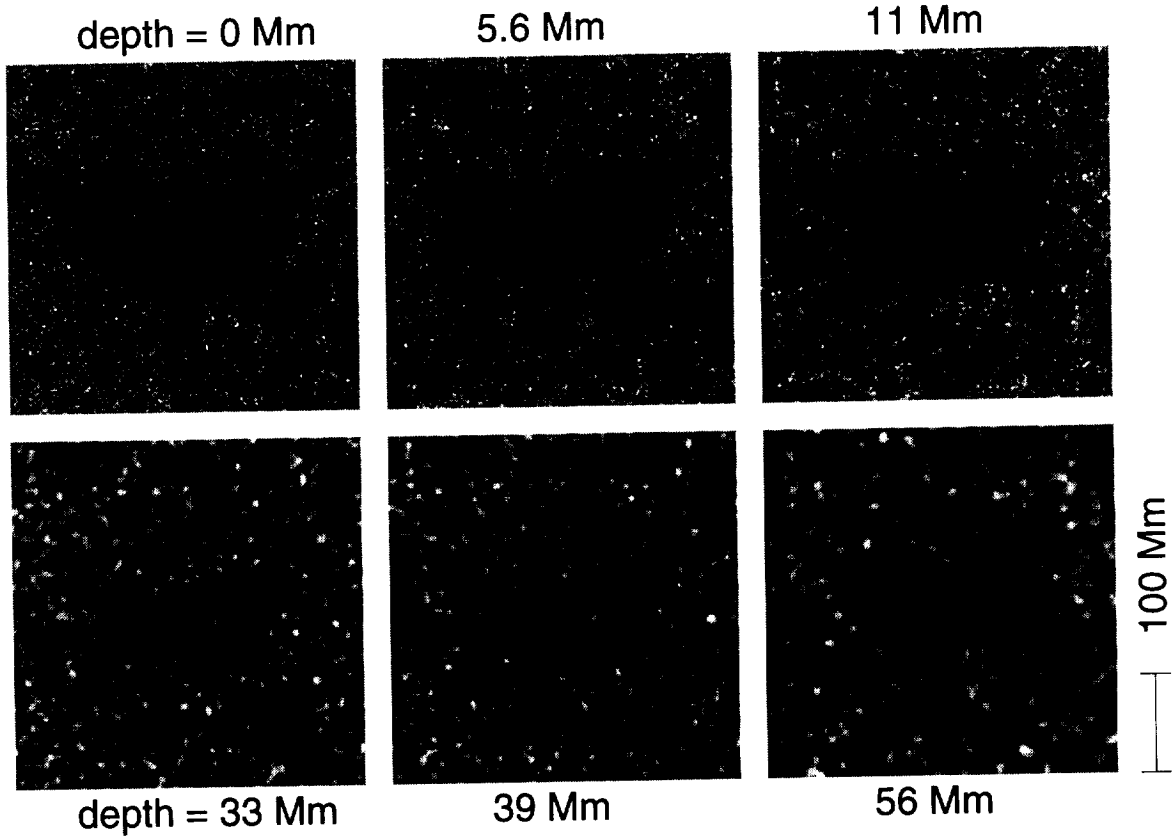

Figure 1: Holographic images of artificial seismic noise that encounters alphanumeric absorbers just beneath the surface and at a depth of 56 Mm. Each frame shows the regressed acoustic power at a focal-plane depth indicated above or below.

Lindsey et al. (1996) elaborate on the analogy between seismic holography and the function of standard lens optics in the electromagnetic domain. The eye derives all of its information about the outlying world from nothing more than the electromagnetic field at the surface of the cornea. Helioseismic holography does much the same with acoustic

disturbances measured at the solar surface, extrapolating them backwards into the solar interior to render acoustic images of sub-photospheric features that have contributed to them. Except that this extrapolation is accomplished computationally, it is otherwise strongly analogous to that of standard optical holography. The analogy between familiar optical holography should be clear when one reflects that the function of mixing light scattered from the subject with a reference beam is to secure phase information onto a photographic plate, which is normally sensitive only to amplitude. In the case of familiar optical holography, the interference that renders this phase information requires macroscopic coherence lengths, thus monochromatic radiation. Applying a monochromatic beam through the hologram from the reverse direction can be interpreted as using the hologram to drive the vacuum on its subject side to produce an electromagnetic field that condenses coherently back to the location formerly occupied by the scatterer. Solar seismic holography simply accomplishes this computationally, but over a broad band, since the helioseismic observations contain full phase information over all frequencies. Computational seismic holography is *not* an approximation based on ray optics nor does it compromise in any way on strict obedience of solar interior acoustics to wave mechanics. Like its electromagnetic counterpart, seismic holography *is wave optics* and as such contains a full account for the effects of diffraction. As such, seismic holography is subject to the same fundamental limitations in terms of diffraction and statistics as any other diagnostic based on helioseismic observations. It is likewise open to the full range of standard optical techniques that have been developed to optimize the informational content of coherent electromagnetic radiation.

Figure 2 shows a working example of seismic holography applied to SOHO-MDI observations, taken from Lindsey and Braun (1998). The images compare the 6 mHz holographic signature of a single sunspot (left column) with "egression power maps" of localized superficial absorbers in a plane parallel acoustic model illuminated by a random, isotropic noise spectrum (right column). The model renders an assessment of the sensitivity of focus with respect to depth. The persistence of the signature several Mm beneath the absorber in the model, an artifact which we call the "acoustic stalactite", suggests that the egression signature of the visible sunspot, is roughly consistent with absorption that is entirely superficial. A conspicuous satellite appears north-east of the sunspot, indicated in the left column by arrows. This signature persists to a depth of 11.2 Mm, at which the stalactite attached to its superficial counterpart in the model has spread to a diffuse annulus. This is not discernible to the eye but is the reason for the significantly negative contrast (see plot at below right).

It is important to recognize that the signatures appearing in the shallower focal planes in Figure 1 are *not* a representation of acoustic disturbances that have propagated directly upward to appear directly in the neighborhood of the sources from which they emerged. They are rather a representation of acoustic radiation that was emitted *downward* and refracted back to the surface many Mm away from the focal point, $\mathbf{r}$, of the computation. The signature seen at depth zero (Fig 1a) is therefore the solar photosphere imaged *through* the solar interior by waves that have traveled up to 20 Mm beneath it before being refracted back to the solar surface up to 45 Mm away.

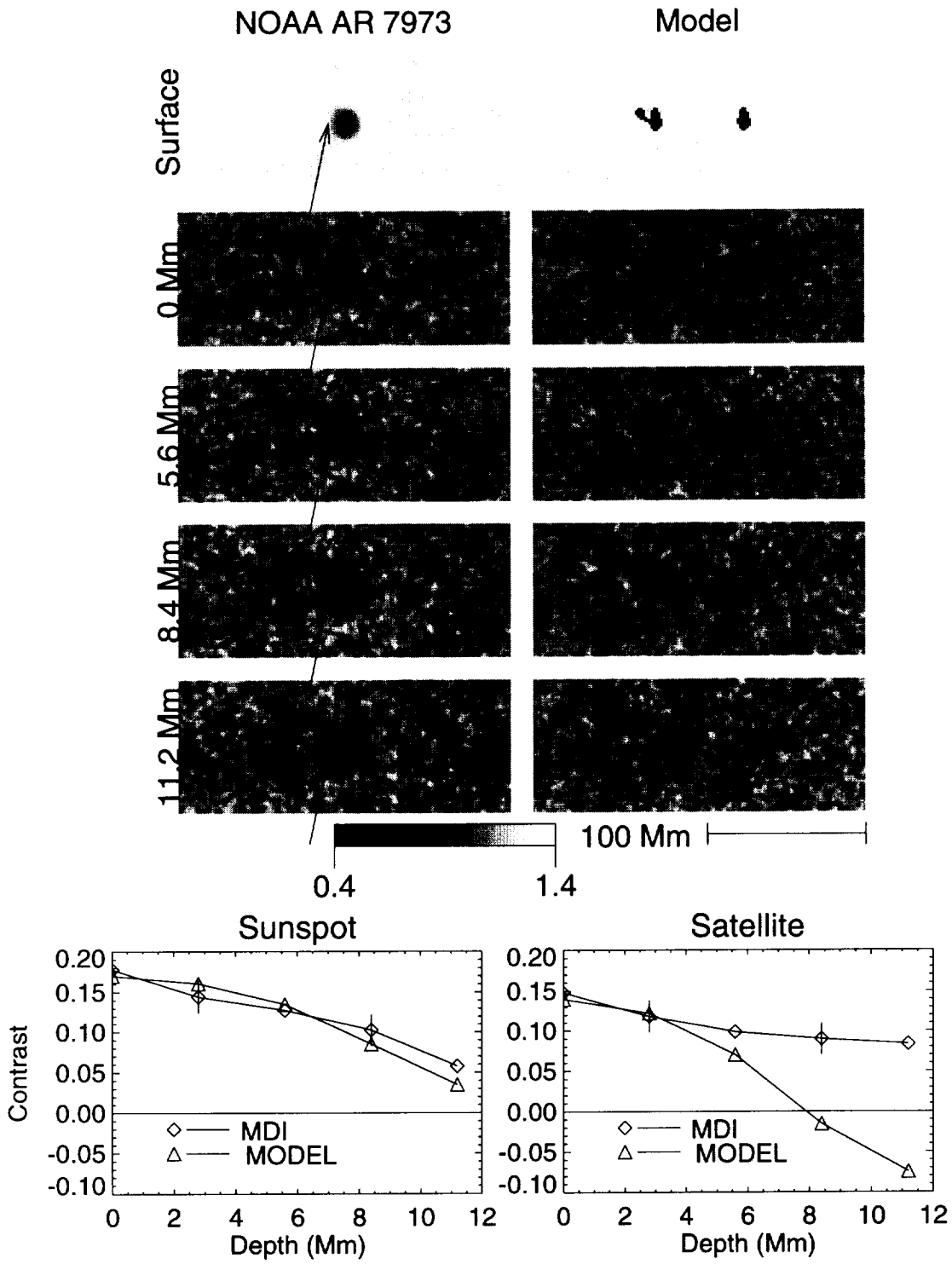

Figure 4: Egression power maps (left column) of NOAA AR 7973 integrated over 24 hr on 1996 June 25 in 6 mHz acoustic radiation (1 mHz bandwidth) with focal planes ranging from the surface to a depth of 11.2 Mm. The right column shows respective egression power maps of acoustic noise propagated by a Christensen-Dalsgaard model locally depleted by a superficial absorber intended to match the primary signature in the upper left egression map. Arrows in the left column locate a satellite of the primary acoustic deficit signature in each frame of the upper row that extends well below the acoustic stalactite that represents its superficial counterpart in the left column. High-resolution contrasts of the sunspot were computed by comparing the egression power averaged over a small disk (radius 8.4 Mm) and the west side of a surrounding annulus, to avoid the satellite. This is plotted in the lower left box of the Figure. A similar contrast is computed for the satellite (radius 8.4 Mm) and plotted at lower right.

"Acoustic condensations" such as that represented by the satellite that appears in Figure 2 appear occasionally in 5–6 mHz egression-power images in focal planes up to 20 Mm in depth. Figure 3, taken from Braun and Lindsey (1999a) shows some further examples. Arrows a, b, and c in Figs 3b, 3c, and 3d point to condensations that appear in the respective frames in which they are labeled. The egression power maps invariably show acoustic stalactites persisting to great depths directly beneath strong absorbers at the surface.

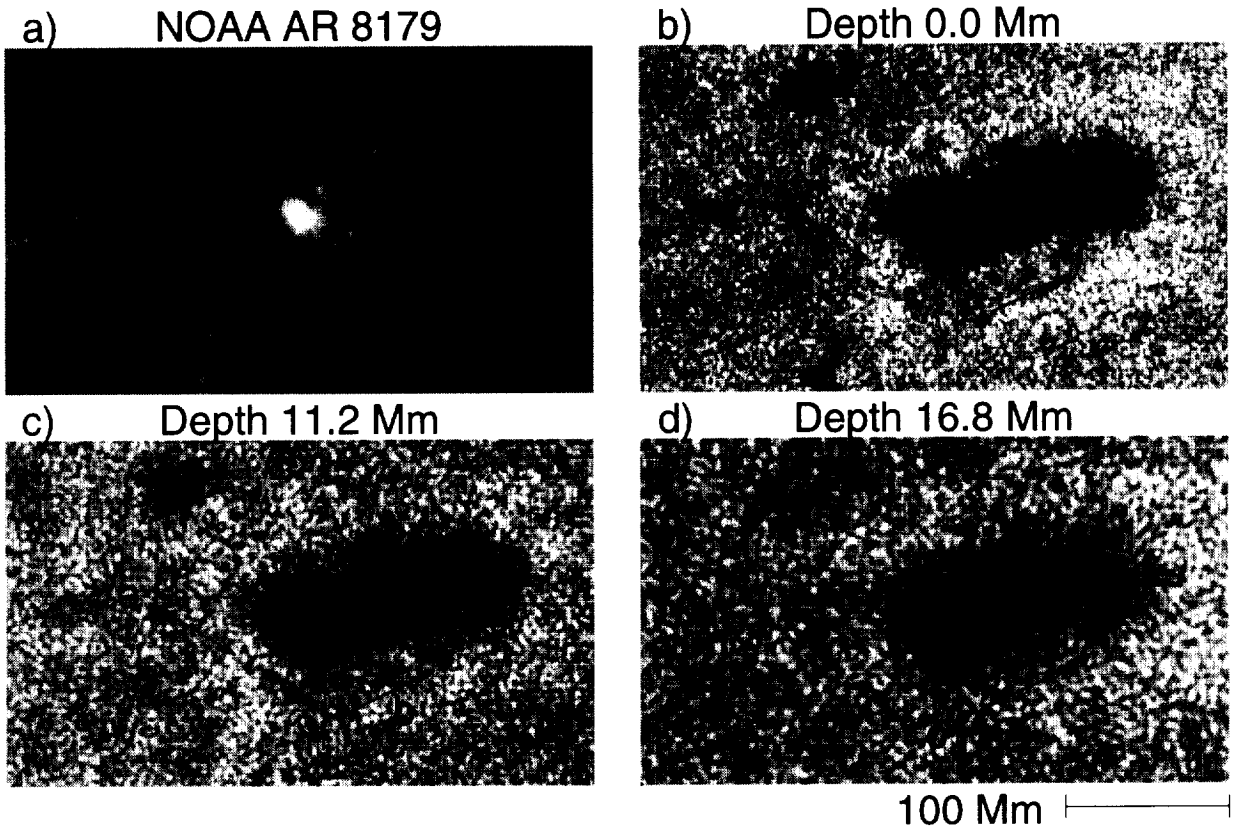

Figure 3: Egression power maps at 5 mHz (1 mHz bandwidth) of NOAA AR 8179 integrated over a 24 hr beginning at 1998 March 16.0 are shown in focal planes at the surface (Frame b), and at depths of 11.2 Mm (Frame c) and 16.8 Mm. Frame a shows a magnetogram of the region. Arrows a and b indicate condensations that emerge at a depth of 11.2 Mm (Frame c). Arrow c indicates condensation that appears at a depth of 16.8 Mm.

Practical models of complex distributions of acoustic perturbations require a careful account of these artifacts. Due to considerations related to diffraction, acoustic stalactites eventually impose fairly rigid limitations on depth discrimination. These limitations are fundamental and apply to any seismic diagnostic in rough proportion to its vulnerability to the effects of diffraction. Nevertheless, acoustic stalactites can be can be minimized by a well appropriated holographic computation that takes full advantage of a generous computational pupil, and these are amenable to modeling based on relatively simple deconvolution techniques. Because of the severe diffraction effects that encumber non-holographic tomography and the tentative indication to the contrary by the best ap-

propriated holographic images we have obtained to date, we are presently most inclined to doubt that actual physical perturbations beneath active regions conform to the conspicuously vertical guidelines which some authors have claimed based on other seismic analyses.

1.2 *RESULTS OF OUR RESEARCH*

The general technique we introduced under the term "helioseismic holography" was also proposed years before by Roddier (1975). Chang et al. (1997) applied the technique in the time-distance perspective to some 90 hr of observations from the Taiwan Oscillations Network (TON) to obtain the first holographic detection of acoustic absorption by sunspots. This phenomenon was discovered some ten years before by Braun, Duvall and LaBonte (1988) by the now familiar "Hankel analysis", which easily renders the effect in an 8 hr timeseries of seismic observations. In fact, a well appropriated holographic reconstruction applied to high-quality helioseismic observations clearly renders the acoustic deficit associated with a moderately large sunspot with a temporal resolution of less than 10 min. In the past two years, seismic holography has proceeded to uncover a remarkable array of solar acoustic phenomena that had hitherto been undiscovered, and resolved a number of puzzles that had been posed by previous diagnostics. All of these major discoveries to date (those of which we are both aware and substantially convinced) have come out of the SOHO-MDI database.

1.2.1 The Acoustic Moat

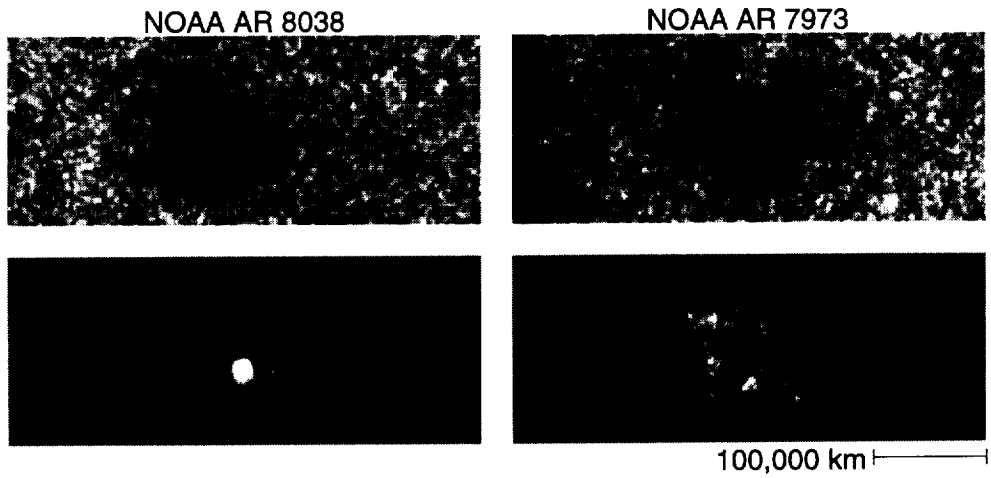

Figure 4: Egression power maps of acoustic moats surrounding sunspots in actives regions NOAA AR 8038 on 1997 May 10 (upper left) and NOAA AR 7973 on 1996 June 25 (upper right) are shown above respective Kitt Peak magnetograms. The egression power maps are each integrated over the 2.5–3.5 mHz frequency band for a 24 hr period. The lower row of frames show the evolution of the acoustic moat surrounding the sunspot in NOAA AR 7973 from 1998 June 23 (right) to June 26 (left).

A remarkable result of Braun et al. (1998) was the discovery of the "acoustic moat", a region showing a general acoustic deficit of 10–30% in 3–4 mHz acoustic radiation surrounding all well-developed sunspots, with radii in the general range 30–60 Mm. The region defined by the acoustic moat correlates to some degree with surrounding plage,

but tends to be more contiguous. The acoustic moat often extends into regions that are magnetically quiet. Examples are shown in Figure 3, taken from Braun & Lindsey (1999c). Upper frames show maps of 3-mHz egression power integrated over 24 hr of NOAA AR 8038 on 10 May 1997 (upper left) and NOAA AR 7973 on 25 June 1996 (upper right), above respective concurrent NSO magnetograms from the Kitt Peak Vacuum Telescope.

Braun et al. (1998) caution against the assumption that the acoustic moat has its own absorption mechanism, suggesting that it simply scatters the acoustic deficit introduced by the sunspot itself. They propose that the acoustic moat signifies an anomalous convection cell flowing rapidly outwards not far beneath the solar surface, driven by heat accumulation caused by the blockage of convective transport through the sunspot photosphere. Evidence that the acoustic deficit of the moat is predominantly a scattering phenomenon is not entirely conclusive at this point, but is beginning to be quite strong.

1.2.2 Acoustic Glories

Holographic images of some active regions, particularly growing multipolar magnetic regions, show a halo of excess 5–6 mHz seismic emission that is quite conspicuous. At 5 mHz these "acoustic glories" often contain small seismic emitters that tend to congeal in strings. A clear example appears in Fig 3b. Donea, Braun and Lindsey (1999) show that the small emitters that characterize acoustic glories at 5 mHz are nearly all confined to the quiet Sun, usually bordering weak magnetic regions and sometimes marking the neutral line between positive and negative polarity The individual emitters which they examined tended to sustain a continuous excess in emission, remaining stationary for periods of 10–20 hours as the outer boundary of the active region expanded outward towards it.

1.2.3 Phase Sensitive Holography

Lindsey and Braun (1997) introduced the concept of phase-sensitive holography as a means of imaging a broad spectrum of possible perturbations that scatter or refract acoustic radiation without absorbing it. These sources would be invisible to simple acoustic power holography in an acoustic field that is isotropic. Phase-sensitive holography is very similar, in principle, to Schlieren imaging. In the spectral domain, it is accomplished directly by phase-correlating the ingression with the egression. Phase-contrast holography at 3 mHz shows a uniformly strong correlation map for surface correlations over the quiet Sun, because the quiet photosphere reflects the ingressing spectrum specularly, preserving the horizontal wavenumber, l, of the mode. Sunspots, plages, and acoustic moats invariably render significant phase shifts consistent with reduced travel times.

Figure 5 shows phase-sensitive holography in 3 mHz radiation of NOAA AR 8179, the same region shown in Figure 4, above, in 5 mHz radiation. Fig 5b shows the extended, diffuse signature of the acoustic moat that appears in egression power. Fig 5c shows a map of time delays equivalent to the phase-shift of this signature, the argument of the correlation between ingression and egression.

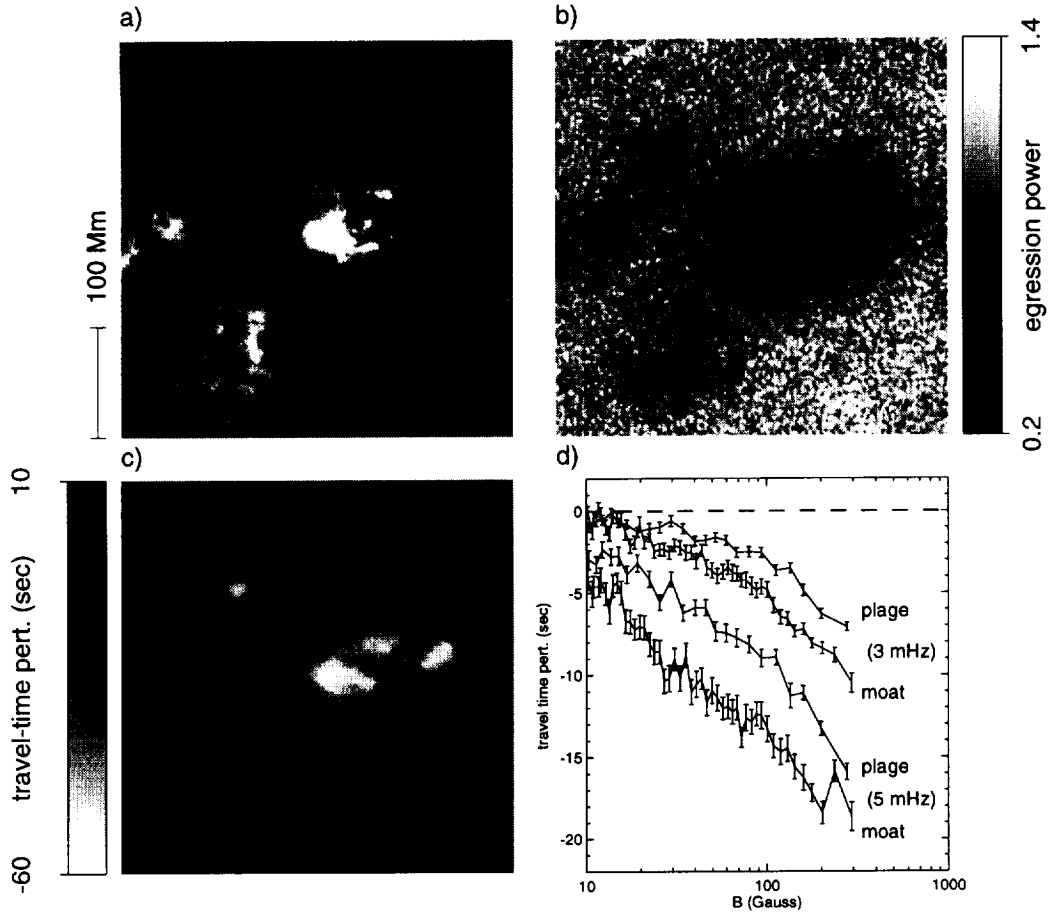

Figure 5: Phase-sensitive holography of NOAA AR 8179, integrated for 24 hr beginning at 1998 March 15.0. Figs 5a and 5b show show, respectively, a SOHO magnetogram and a 3 mHz egression power map of the region. Fig 5c shows a map of travel time perturbations determined from the phase of the egression-ingression correlation. Fig 5d compares 3 mHz and 5 mHz travel-time perturbations for plages in acoustic moats with naked plages far from sunspots.

Unlike the egression power signature, the phase perturbations seem to be correlate strongly with surface magnetic regions. Braun and Lindsey (1999b) propose to interpret these reduced travel times in terms of an "acoustic Wilson depression" that applies to all surface magnetic regions. Phase-sensitive holography at just the surface by itself cannot readily distinguish between a Wilson depression and a sound-speed enhancement in an underlying acoustic moat, either of which reduces sound-travel times. That the contribution of the acoustic moat is also significant is nevertheless clearly seen by comparing phase perturbations of magnetic regions in acoustic moats with magnetic regions in isolated, naked plages. These statistics, shown in Fig 4d, characterize acoustic moats with time delays of order 5–10 s. The phase perturbation contributed by the acoustic moat might be explained by a thermal excess due to the blockage of convective transport by the underlying sunspot photosphere. Braun and Lindsey (1999b) present statistics to suggest that the entirety of the frequency shifts of global modes with the solar cycle can be explained by the superficial phaseshifts due to plages, acoustic moats, and sunspots, in order of estimated importance.

There is now tentative evidence that the signature of the acoustic moat in egression power is predominantly a result of Doppler scattering. It is the Doppler signature that most appears to reflect the extended, diffuse, non-plage-like appearance of the egression-power signature of the acoustic moat. Figure 6 shows the horizontal Doppler signature of the quiet-Sun supergranulation (Fig 6a) and a sunspot (Fig 6b, NOAA AR 8243). These are preliminary, uncalibrated results computed according after Lindsey and Braun (1997). Outflows surrounding sunspots are already the subject of a large volume of literature based on magnetic tracers and surface Doppler measurements, and this interpretation agrees with the earlier helioseismic diagnostics reported by Lindsey et al. (1996). The preliminary results reported show no evidence of the massive inflows that would be needed to explain the 1–2 km/s downflows that Duvall et al. (1996) and some others have generally inferred beneath sunspots based on time-distance correlations.

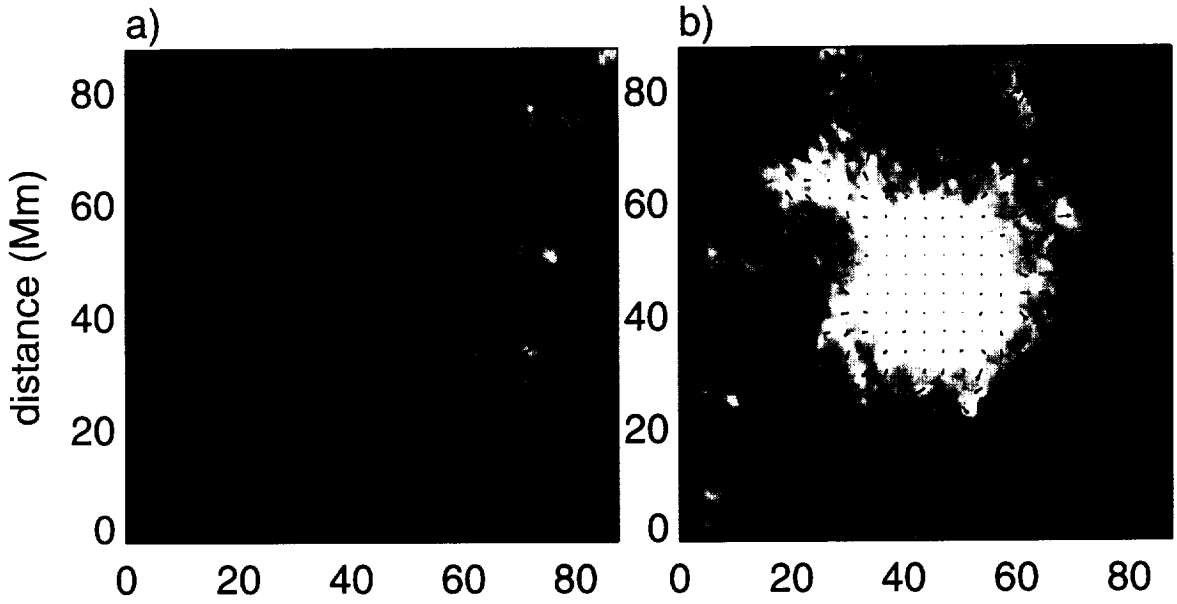

Figure 6: Horizontal Doppler holography, as prescribed by Lindsey and Braun (1997) and applied to high-resolution SOHO-MDI observations of NOAA AR 8243 and its surroundings, shows horizontal flows associated with the supergranulation (Fig 5a) and outflows surrounding a sunspot (Fig 5b).

1.2.4 Other Developments

Seismic holography has given us the first images of a solar flare with some remarkable results, for which we simply refer to Donea, Braun and Lindsey (1999). Comparative 1- and 2-skip egression-power images of sunspots clearly show the strong dependence of the reflectivity of the quiet photosphere on frequency, ν (Lindsey and Braun 1998). More recent applications to the high-resolution MDI images are now showing us the weaker, but significant, dependence on the spherical harmonic degree, l. Phase-sensitive holography of active regions have also now shown us that active-region subphotospheres are strongly reflective, in contrast to the quiet Sun, which acts as a nearly perfect absorber at these frequencies (Braun & Lindsey 1999b). Donea, Lindsey and Braun (1999) have found that the distribution of 5 mHz seismic power from acoustic glories significantly saturates above $\sim$6 times the quiet Sun mean, as opposed to a quiet-Sun distribution

that can be characterized as Gaussian noise. This may help us to understand the mechanisms of acoustic emission from the near subphotosphere.

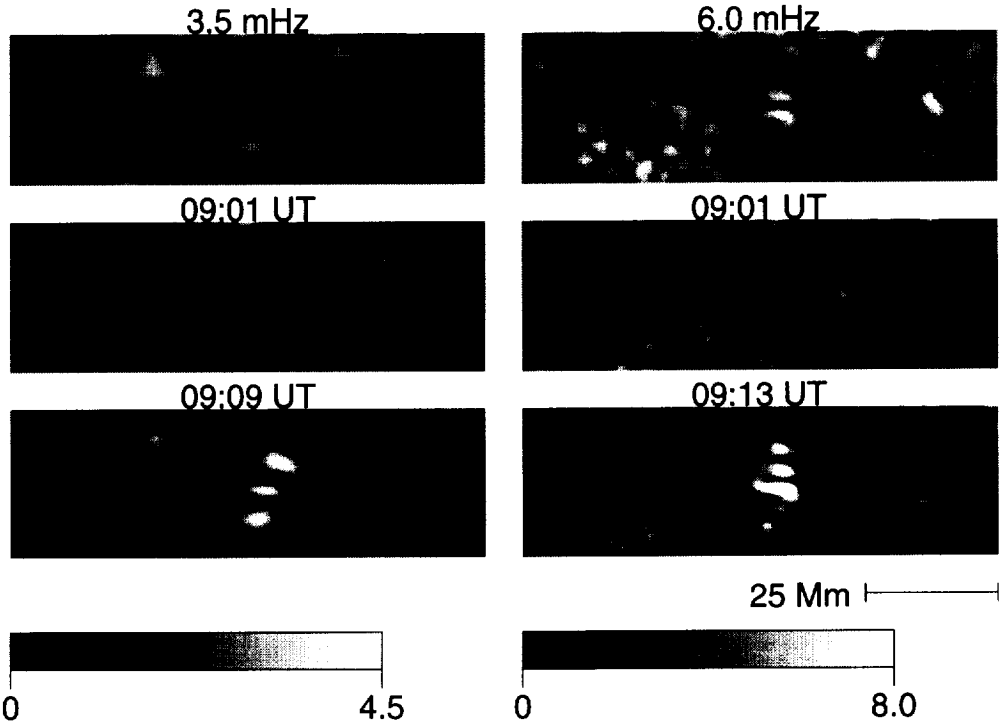

Figure 7: Egression-power images of the solar flare of 1996 July 9 in NOAO AR 7978 in 2 mHz bands centered at 3.5 mHz (left column) and 6 mHz (right column), taken from Donea, Braun & Lindsey (1998). The onset of the flare is approximately 09:07 UT. Upper frames show the egression power integrated over a 2 hr period beginning at 8:06 UT. Middle frames show the instantaneous square modulus of the egression minutes before flare onset, which represents an integration over 500 s as a result of truncation of the frequency band of the computation to 2 mHz.

1.3 *SUMMARY*

The recent advent of local helioseismology is now allowing us the first clear view into the near solar interior from a local perspective, giving us high-quality images of acoustic perturbations beneath active-region photospheres and sunspots. Solar acoustic holography is already giving us much needed insight into the problem of thermal transport in the neighborhoods of sunspots. It is showing us compelling evidence of subsurface acoustic perturbations up to 20 Mm beneath active region photospheres (Lindsey & Braun 1998, and Braun & Lindsey 1999a). Seismic holography may make it possible to anticipate the emergence of active regions from deep in the convection zone, or from the far-side surface. Such applications are certain to be of use to us in a 21^{th} century technology to which the behavior of the Sun is critical, by its influence on satellites and in communications technology and space exploration. At the same time, the real technical spinoffs of seismic holography may very possibly remain yet to be discovered. As we could not have anticipated the existence of acoustic glories, the direction in which seismic holography will now take solar research remains unpredictable.

Seismic holography is now opening the near subphotospheres of active regions and the quiet Sun to an understanding from the local perspective that has not been widely

anticipated. It may likewise revolutionize our understanding of the deep convection zone. In so doing, it will certainly contribute to the general advancement of scientific knowledge about the single astronomical entity which we know to be critical to life on earth. The results of this research have numerous potential utilities in the technical domain as well as those that apply to education in the sciences and engineering. Indeed, the technical exercise of peering into the solar interior has invariably held a strong appeal to the younger generation, including the undergraduate and graduate students that come to Tucson for experience in scientific research. This largely accounts for the rapid spread of interest in seismic holography to Europe, the orient and the southern hemisphere. Seismic holography has now become a high-profile topic of all major meetings and conferences on local helioseismology. It is now rapidly becoming clear worldwide that seismic holography is giving us a most extraordinary look into the solar interior. We appreciate that NASA recognized this technique as a powerful solar interior diagnostic and appropriated its support to it before there was widespread awareness of its formidable potential.

1.4 *REFERENCES*

Braun, D. C. and Lindsey, C. 1999a, *Ap. J.* **513**, L79.

Braun, D. C. and Lindsey, C. 1999b, (submitted).

Braun, D. C. and Lindsey, C. 1999c, (in preparation).

Braun, D. C., Lindsey, C., Fan, Y. and Jefferies S. M. 1992, *Ap. J.* **392**, 739.

Braun, D. C., Duvall, T. and LaBonte, B. J. 1988, *Ap. J.* **335**, 1015.

Braun, D. C., Lindsey, C., Fan, Y. and Fagan, M. 1998, *Ap. J.* (in press).

Chang, H.-K., Chou, D.-Y. & LaBonte, B. J. and the TON team 1997, *Nature* **389**, 825.

Donea, A.-C., Braun, D. C. & Lindsey, C. 1999, *Ap. J.* **513**, L143.

Donea, A.-C., Lindsey, C. & Braun, D. C. 1999, *Ap. J.* (submitted).

Duvall T. L., D'Silva, S., Jefferies, S. M., Harvey, J. W., & Schou, J. 1996, *Nature* **379**, 235.

Lindsey, C. and Braun, D. C. 1990, *Solar Phys.* **126**, 101.

Lindsey, C. and Braun, D. C. 1997, *Ap. J.* **485**, 895.

Lindsey, C. and Braun, D. C. 1999, *Ap. J.* **510**, 494.

Lindsey, C. and Braun, D. C. 1998, *Ap. J.* **509**, L129.

Lindsey, C., Braun, D. C., Jefferies, S.M., Woodard, M. F., Fan, Y., Gu, Y., and Redfield, S. 1996, *Ap. J.* **470**, 636.

Roddier, F. 1975, *Compt Rend Accad Sci* **281**, B993.

1.5 *PUBLICATIONS SUPPORTED BY THIS GRANT*

Braun, D. C. & Lindsey, C. 1998, "Helioseismic Images of an Active Region Complex," *Ap. J.* **513**, L79.

Braun, D. C. & Lindsey, C. 1999, "Acoustic Moats" *Ap. J.* (in preparation).

Braun, D. C., Lindsey, C., Fan, Y. & Fagan, M. 1998, "Seismic Holography of Solar Activity," *Ap. J.* **502**, 968.

Donea, A.-C., Braun, D. C. & Lindsey, C. 1999, "Seismic Images of a Solar Flare," *Ap. J.* **513**, L143.

Donea, A.-C., Lindsey, C., & Braun, D. C. 1999, "Stochastic Acoustic Emission from the Quiet Sun and Active Region Environment," *Ap. J.* (submitted).

Lindsey, C., & Braun, D. C. 1998, "The Acoustic Moat and Thermal Transport in the Neighborhoods of Sunspots," *Ap. J.* **499**, L99.

Lindsey, C. & Braun, D. C. 1998, "Acoustic Signatures of Subphotospheric Structure Underlying Sunspots," *Ap. J.* **509**, L129.

Lindsey, C., & Braun, D. C. 1999, "Chromatic Holography of the Sunspot Acoustic Environment," *Ap. J.*, **510**, 494.

Lindsey, C. & Braun, D. C. 1999, "Helioseismic Signatures of Subphotospheric Structure Beneath Active Regions," in *Proc. 1998 SOHO/GONG Workshop* ed. A. Wilson, (Kluwer, Noordwijk) p. 641.

Lindsey, C., & Braun, D. C. 1999, "Phase Sensitive Holography" *Ap. J.* (submitted).

1. A STUDY OF THE PROCESS OF MAGNETIC FLUX DISAPPEARANCE IN CANCELING BIPOLES: K. L. Harvey, H. P. Jones, M. Penn, and D. Hassler

The objectives of this study are two-fold: (1) to determine observationally whether magnetic flux in canceling small bipoles is submerging below the surface or continuing to emerge out through the photosphere; (2) to establish as a function of time the height structure of the magnetic fields, velocity flows, and intensities associated with these small-scale canceling bipoles.

To accomplish these goals, we obtained during three observing campaigns in 1997 and 1998 simultaneous observations of magnetic fields in both the chromosphere and photosphere in collaboration with SOHO/MDI, EIT, and CDS (JOPs 50 and 82), TRACE, and Yohkoh/SXT, the Big Bear Solar Observatory (BBSO), and the High Altitude Observatory at Mauna Loa (HAO). The premise of this observational approach is that if a canceling bipole is submerging, the magnetic flux would disappear in the chromosphere before it did so in the photosphere. Chromospheric and coronal images, as well as other magnetic field observations, would be used to verify this evolution of the magnetic fields.

2.1. *OBSERVATIONS AND DATA PROCESSING*

2.1.1. NSO/KP Observations

The primary data used for this study of canceling bipoles are simultaneous observations of magnetic structures in both the chromosphere and photosphere taken with the same instrument and under the same atmospheric conditions using the spectromagnetograph at the Vacuum Telescope at Kitt Peak (NSO/KP). Called zonal scans, these data are records of the full line profiles of the chromospheric Ca II λ8542 line and of the photospheric Fe I line at 8538Å located in the blue wing of this Ca II line. A example of this spectral region is shown in Figure 1. Both the chromospheric Ca II 8542.1 Å absorption line (g-factor 1.1) and the photospheric Fe I 8538.0 Å absorption line (g-factor 1.225) can be seen along with some fainter atmospheric water vapor lines.

The line profiles were measured at 226 slit positions in both the left and right circular polarization states at each 1.15″ × 1.15″ (September 1997 data) and 2.3″ × 1.15″ pixel (May and June 1998 data) within an area 512 (east-west) by 480 (north-south) arc-seconds (444 × 418 pixels). The observations, repeated at a cadence of 7 minutes, are summarized in Table 1.

For each spectral frame, made at each pixel within the area scanned, several parameters are measured by fitting the Ca II and Fe I line profiles. An IDL software package, developed by M. Penn, was used to determine differences in line-center positions of the absorption lines in the two polarization states yielding maps of the longitudinal magnetic fields for both Ca II and Fe I. While this package worked quite well for the September 1997 observing campaign, it did not for the second two. Application to the May and June 1998 observations showed considerable noise that masks much of the weak magnetic field structure, features in the magnetograms that we need to follow better to accomplish our research goals. We spent some time trying to understand and correct this problem. Penn's method fits the profiles of the core of the Ca II 8542 and Fe I 8538 lines with a parabola and very few sampling points. It is the sparse sampling of the line profile for the fitting that results in the high noise level.

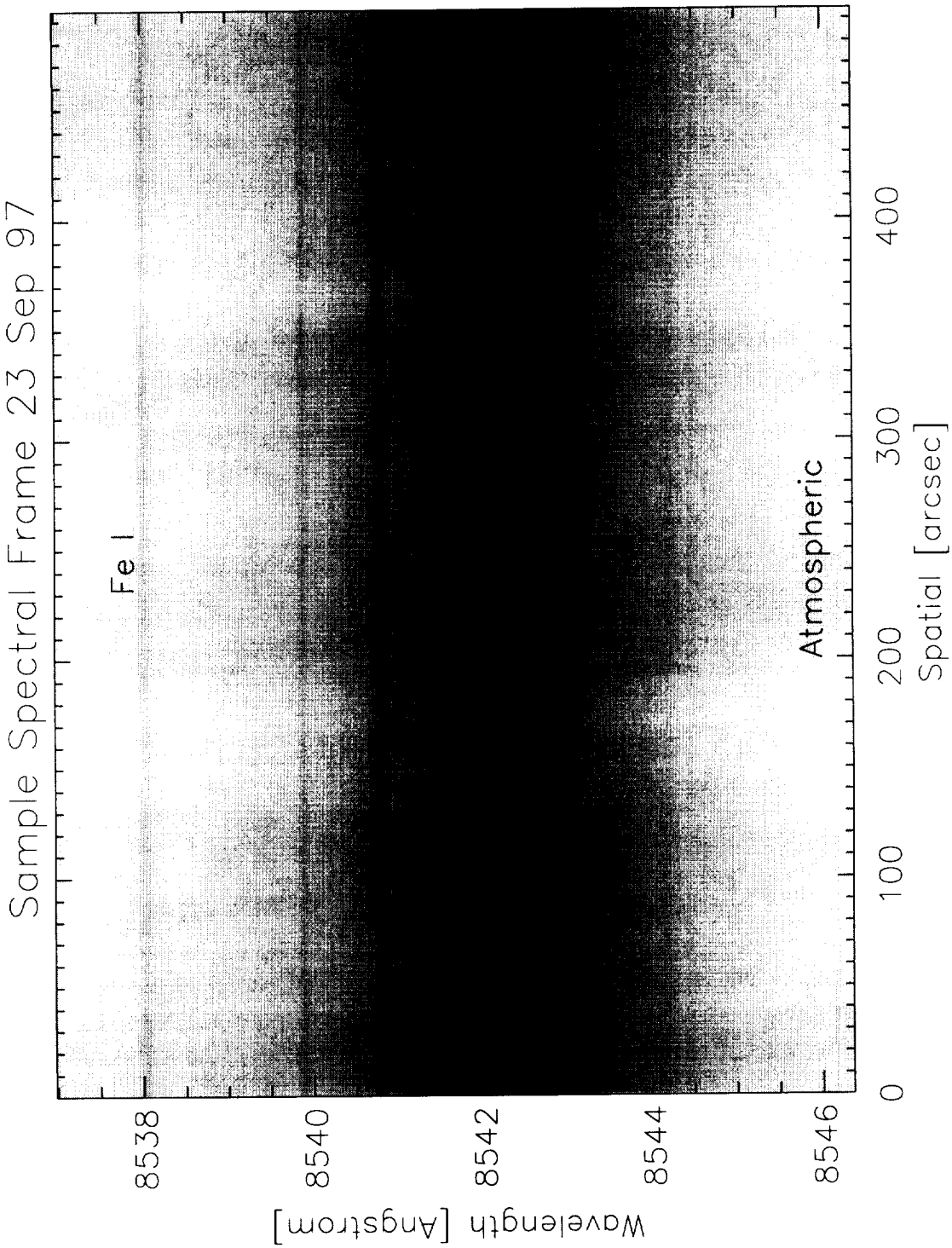

Figure 1. Sample spectral frame from observations on 23 September 1997.

We chose to use a different reduction method developed by H. Jones, also a co-investigator on this project. His method uses a technique similar to that used in reducing the NSO/KP full-disk magnetic observations made with the spectromagnetograph. At every spatial position, the procedure determines the continuum intensity, equivalent width, and wavelength position and intensity of the central minimum (or maximum) of the absorption (or emission) line. The wavelength position of line center is found from a zero-crossing of the convolution of the line profile with a fixed anti-symmetric kernel. This technique can be effectively applied to data taken in the two states of circular polarization to measure the magnetic flux at each pixel. The core of the Ca II 8542 line and the entire line profile of the weaker Fe I 8538 line was used in this process. Jones' reduction programs yielded in a significant reduction in the noise level and a processing time of about 10 minutes per zonal scan compared to the two hours using Penn's routine.

The two sets of magnetograms required some cleaning up to remove streaks, in the case of the Fe I 8538 data, and data spikes. These cleaning procedues involve fitting and removing the streaks with a low order polynomial (generally a quadratic) and the spikes in the data with a median 3×1 filter for the photospheric magnetograms and a 1×3 median filter for the chromospheric magnetograms. The noise in the magnetic field observations is estimated to be about 10 Mx/cm^2 in the Fe I 8538 observations and slightly less (7 Mx/cm^2 for the stronger Ca II 8542 data. As yet, we have no way to clean up the corresponding velocity and intensity measurements; this process will be done in the near future to include these data in the papers to be published on the results of this work.

The output of Jones' routine gives the magnetic flux in units of Gauss, the velocity field in m/s, the line depth in % of continuum, allowing us a direct comparison of the magnetic flux observed at two levels in the solar atmosphere.

A pixel by pixel comparison of the magnetic flux density in the chromosphere and photosphere is shown in Figure 2 for data taken on 4 May 1998. This comparison was restricted to only those pixels located within photospheric magnetic network elements. The scatter plot indicates a reasonable correspondence between the measurements of magnetic flux at the two levels of the atmosphere with a least squares linear fit of $B_{\text{chromosphere}} \sim 0.77 B_{\text{photosphere}}$. This relation is similar to that found for other days in our study.

Important for this study is a determination of the height difference between structures seen in Ca II 8542 and Fe I 8538. Using a VAL Model C atmosphere, Jones (1985, *Australian J. Phys.* **38**, 919) finds that at disk center the Ca II 8542 line main response to fields is at a height of around 1200 km above $\tau_{5000} = 1$. The Fe I 8538 Å line likely forms at or just above the photosphere (~200 km).

2.1.2. Collaborating Observations

During the September 1997 observing campaign, the NSO/KP magnetic field data acquisition was coordinated with observations taken with three of the SOHO instruments (MDI, EIT, and CDS), the Yohkoh/SXT instrument, and at several ground-based observatories (BBSO, NSO/SP, HAO/CHIP, Helio Res.). For the May and June 1998 runs, TRACE joined in this collaboration.

The SOHO observations include EIT images in He II 304Å, Fe XII 195Å, and Fe IX/X 171Å full-disk images, along with high-resolution (2.5″ pixels), restricted-area images in He II 304Å of the target area. MDI high-resolution (0.6 ″ pixels) magnetograms and CDS images

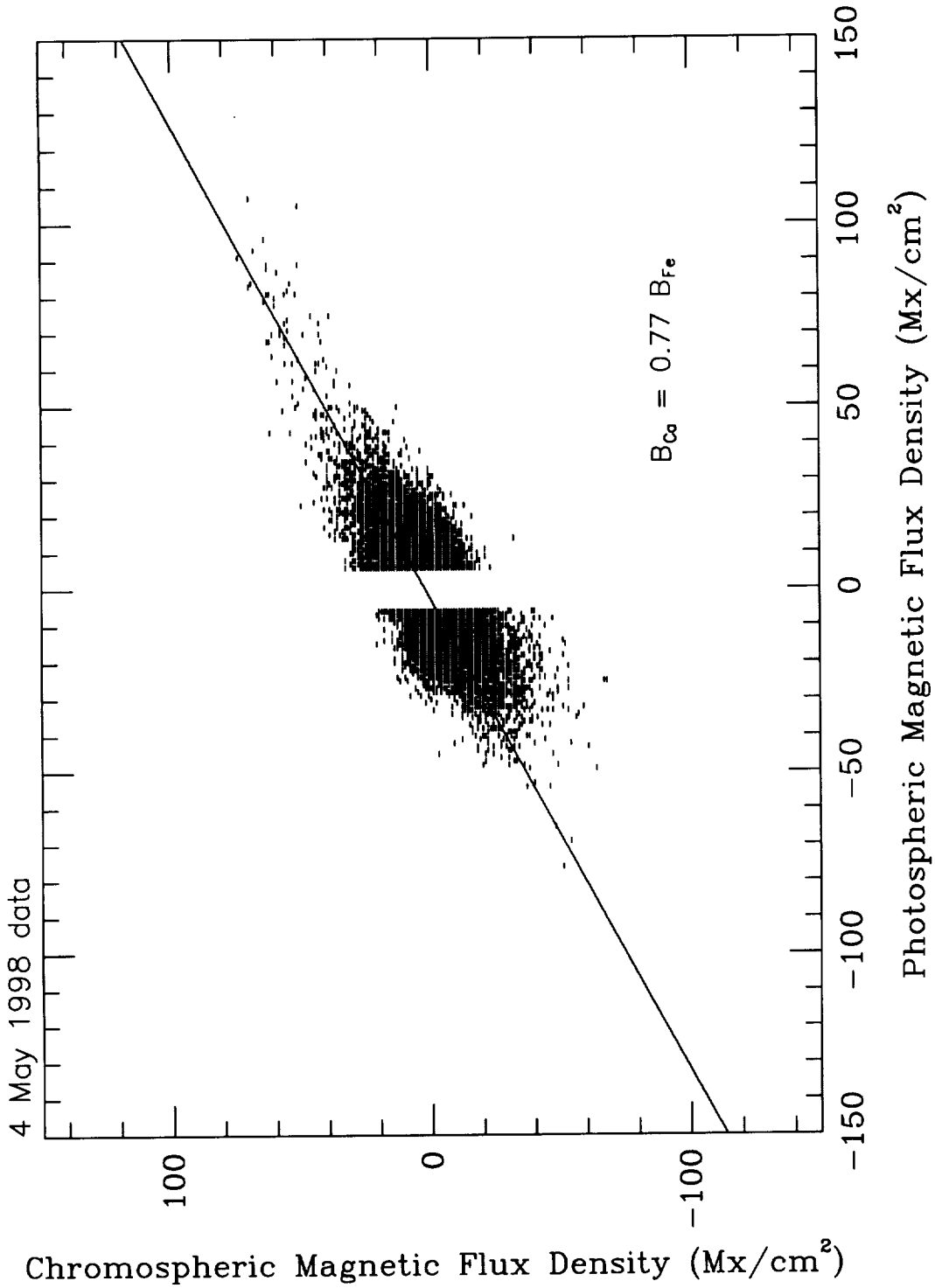

Figure 2. Scatter plot of magnetic flux density in photosphere compared with that in chromosphere. The fit is a least squares linear curve of the form indicated in the lower right of the plot.

made in several EUV lines. Yohkoh/SXT observations include 5 arc-minute square images of the target with a spatial resolution of 5″, as well as full-frame images. TRACE made high-cadence observations (~2 minutes) in Lyα, Fe IX/X 171 Å and FeXII 195 Åwith a spatial resolution of 2″. Ground-based data include Hα filtergrams in line center and in the wings, photospheric magnetograms, and He I 10830Å full-disk filtergrams.

Table 1. Times of NSO/KP Observations: May 1998

Date	Times (UT)	# of Scans	Center Position
1997			
18 Sep	1840–2145	27	N10.6E00
19 Sep	1705–2147	40	N10.6E00
20 Sep	1659–2115	26	N10.6E00
22 Sep	1834–2201	25	N10.6E00
23 Sep	1817–1928	11	N10.6E00
1998			
4 May*	1720–2300	42	N04E00
5 May	1953–2325	30	N04E00
6 May**	1516–2100	44	N04E00
14 Jun*	1554–2309	57	N04E00
15 Jun*	1549–2215	52	N04E00
16 Jun*	1612–2223	50	N04E00
17 Jun**	1516–2100	44	N04E00

* days included in analysis
** not included due to clouds

2.1. *DATA ANALYSIS AND RESULTS*

2.2.1. NSO/KP and SOHO Observations

For this investigation, we have concentrated on processing and analyzing those days that are relatively cloud-free and with durations of 5 to 6 hours in order to maximize the chances of detecting the complete cancelation of several bipoles. These dates include four days: 4 May 1998 and 14–16 September 1998 (see Table 1).

Figure 3 shows the area and its position targeted by the NSO/KP spectromagnetograph relative to the full-disk during one day in the last campaigns. For all of the collaborative campaigns, we selected disk center for observation for two reasons: first, the equatorial regions of the Sun were quiet at this time in the rising phase of cycle 23. We were interested in obsrving areas of quiet sun; and second, to simplify the interpretation of the chromospheric magnetic field observations. At disk center, there is less problem with spatial displacements due to the height difference between the fields observed at these two levels in the atmosphere than if we were observing close to the limb.

The first part of our analysis involved a survey of the four sets of time-sequence mag-

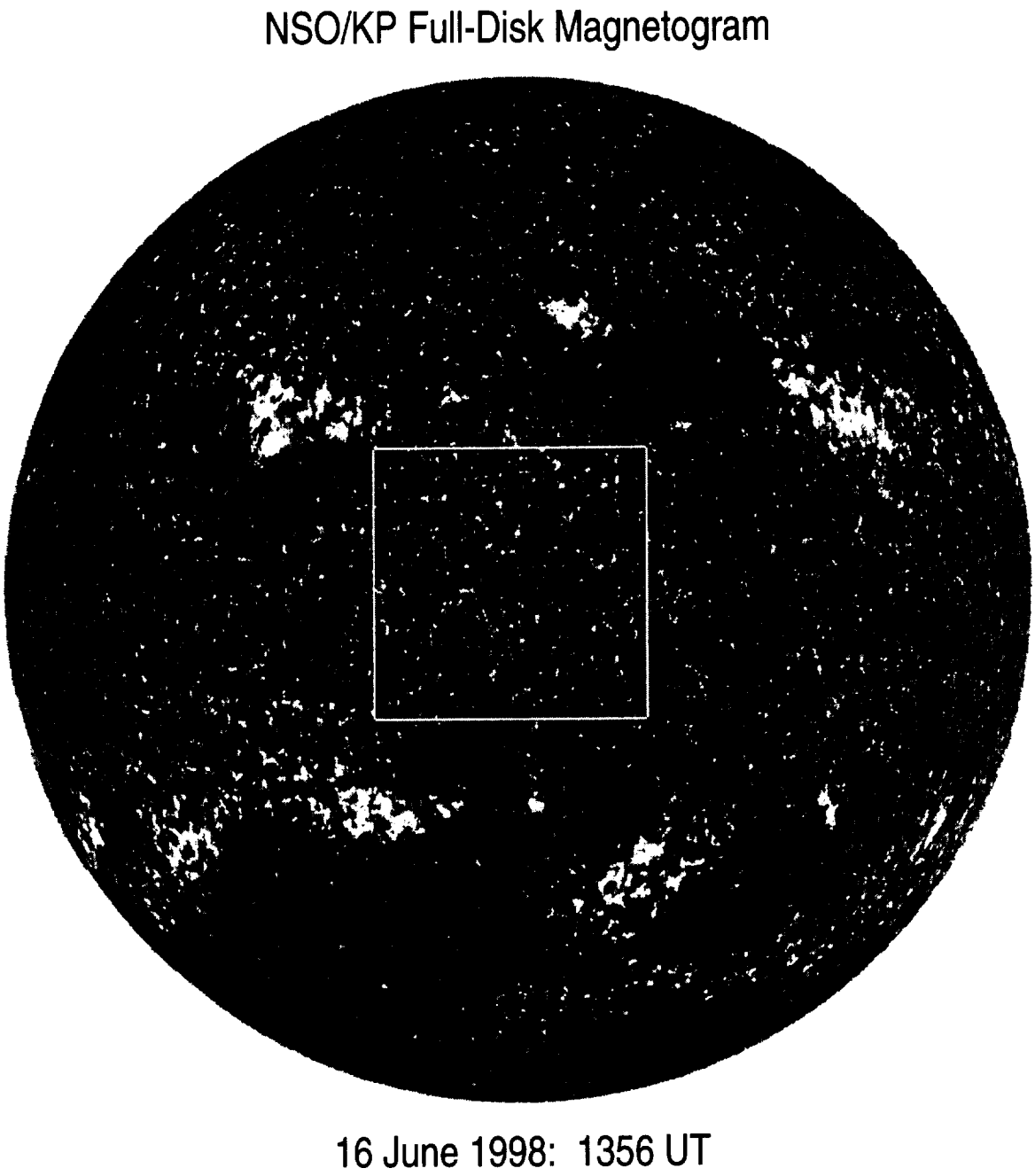

Figure 3. NSO/KP full-disk magnetogram on 16 June 1998 with the area covered by the NSO/KP zonal scans outlined in white. The positioning of this area relative to disk center is the same for all of the observing campaigns.

netograms separately for the chromosphere and photosphere. Seeing variations and noise in the data indicated that an aid to this survey would be to smooth the data by averaging three (3) sequential magnetograms. This eliminated the 5- and 3-minute oscillations seen in both the photospheric and chromospheric magnetograms, apparently a result of some cross-talk of the velocity in the solution of the magnetic signal. This is one aspect of the processing that will be looked into re-evaluting the magnetic field processing before publishing the results of our study in the near future. The chromospheric magnetograms often showed the evolution of bipoles and the network better than the more noisy photospheric magnetograms. It is for this reason that our analysis needs to include chromospheric and coronal images to verify the behavior of the NSO/KP magnetic field observations.

Table 2. Results of Survey of NSO/KP 1998 Magnetograms

	Number of Canceling Bipoles				# Emerging
Date	nc*	P > C	P ~ C	C > P	Bipoles
4 May	3	6	3	2	3
14 Jun	1	3	3	1	6
15 Jun	4	5	8	4	3
14 Jun	0	6	1	1	2
Total	8	20	16	9	14

* bipole did not completely disappear during observations
P, C indicate timing of disappearance of photospheric and chromospheric flux

In this survey, we identified the sites of both canceling and emerging bipoles. The later bipole evolution provided a comparison to the behavior of canceling bipoles at both levels of the atmosphere. A total of 53 canceling bipoles and 14 emerging bipoles were found (see Table 2). Of the 53 canceling bipoles, 45 (85%) disappeared within the time frame of the observations.

For 16 (35%) of the 45 canceling bipoles that disappeared during our observations, the observed magnetic flux in the chromosphere and photosphere disappeared at the essentially the same time. The inability to resolve the evolution in height may be a result of a combination of the time resolution of our observations (14 minutes) and the noise in the data. A magnetic structure, for example, moving vertically at 1 km/s would traverse about 850 km in 14 minutes; this distance is nearly the height difference between the two lines we are observing.

In 20 of the 45 canceling events (44%), we could clearly detect a significant difference in the timing of the apparent completion of the cancelation process between the two levels of the atmosphere in the sense of the magnetic flux in the chromosphere disappearing before the magnetic flux in the photosphere. One such example is shown in Figures 4 and 5. The canceling bipole, indicated by the arrow, was seen in the full-disk magnetogram taken 2 hours earlier was a larger bipole with significantly more magnetic flux. By the time the zonal scans

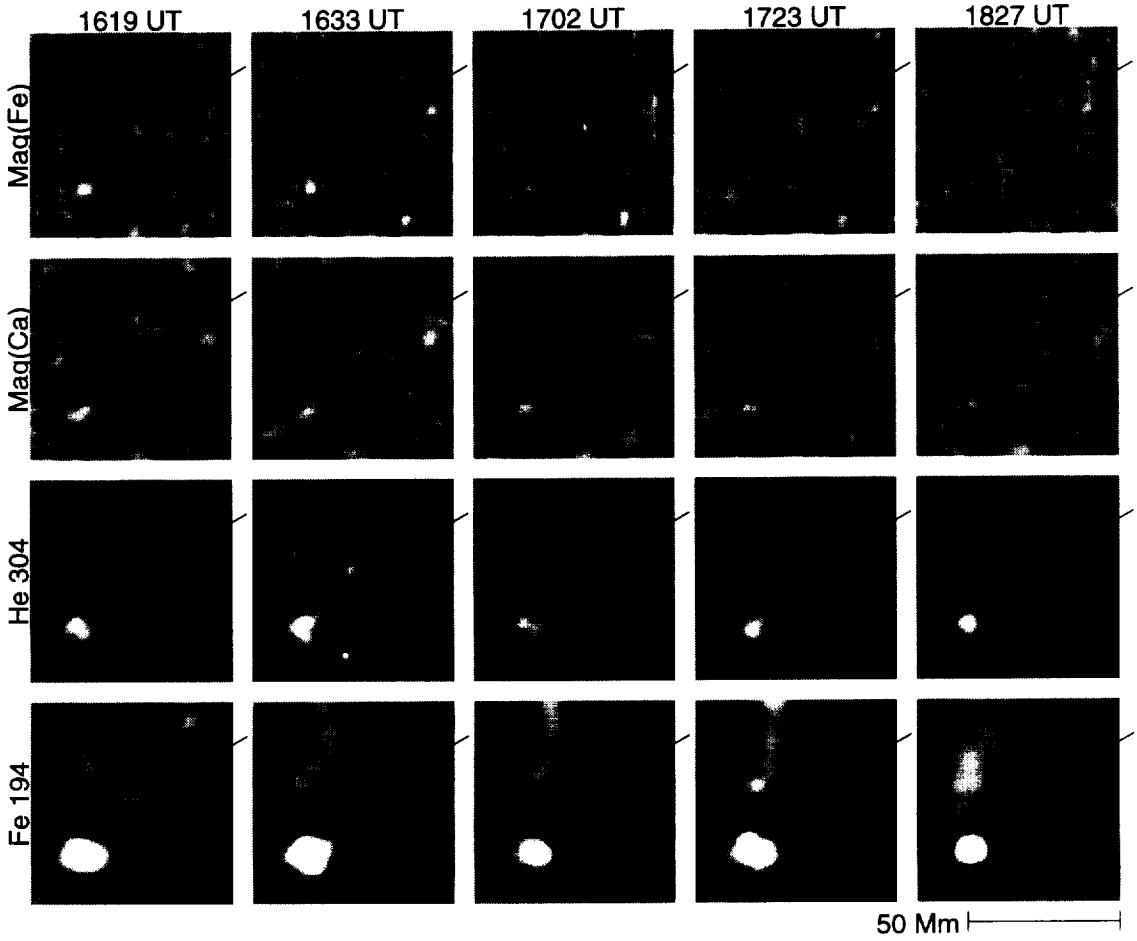

Figure 4. Section of the photospheric Mag (Fe) and chromospheric Mag (Ca) magnetograms of a canceling bipole *(at arrow)* observed on 16 June 1998. Note the disappearance of the positive (white) pole earlier in the chromosphere than in the photosphere. The bottom two sets of panels show the corresponding EIT images in He II 304 Å and Fe XII 195 Å. The times of each vertical column of images is indicated at the top.

began at 1612 UT the magnetic bipole was the canceling bipole had a dimension along its magnetic axis of 9500 km in the photosphere and 8300 km in the chromsophere. The images in Figure 4 show the disappearance of the positive (white) pole in the chromosphere several frames before it is gone in the photospheric observations. This is shown graphically in Figure 5 where the positive magnetic flux in this canceling bipole is gone in the chromosphere by 1740 UT and by 1845 UT in the photosphere, an hour later. This behavior is confirmed by the EIT observations in corona (Fe XII 195 Å) and chromosphere (He II 304 Å). The associated coronal bright point disappears between 1635 and 1651 and the enhanced chromospheric structure between 1722 and 1737 UT. This latter time is consistent with the disappearance of the chromospheric magnetic structure. Spatially, the coronal bright point is smaller than the associated chromospheric structure, overlying the polarity inversion of the canceling bipole. The enhanced He II 304 chromospheric structure is associated with each pole of the magnetic bipole and gets smaller with time. This general evolution of the magnetic and intensity structures at several heights in the atmosphere is typical for the other 19 cases of canceling bipoles. The time delays for the disappearance of magnetic flux at the two levels of the atmosphere range from 15 to 65 minutes, with an average delay of about 35 minutes. If the time delay between the disappearance of magnetic flux in the chromosphere and photosphere can be attributed to the submergence of magnetic flux below the photosphere, as the above observations strongly suggest, the vertical speed of decent of the magnetic flux is about 0.5 km/s. This velocity is similar to the horizontal approach velocity individual opposite polarity magnetic elements involved in the canceling bipole.

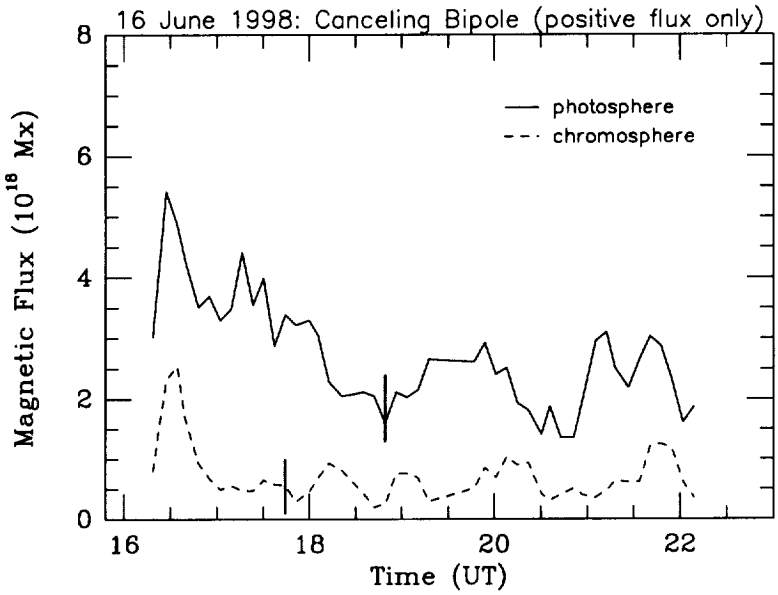

Figure 5. Plot of the positive flux in the canceling bipole shown in the previous Figure. The vertical bars indicate the respective times of disappearnce of the positive flux based on a polynomical fit to the data.

For 9 of the canceling bipoles, the chromospheric magnetic flux was observed to disappear after that observed in the photosphere. Because the photospheric magnetic field data is noisier than the chromospheric data, it is not clear at this time, if these events represent mag-

netic flux the is rising up through the atmosphere. We need to do a detailed comparison with other data, such as the chromospheric and coronal images and photospheric magnetograms, to verify the timing of the disappearance at these two levels in the atmosphere.

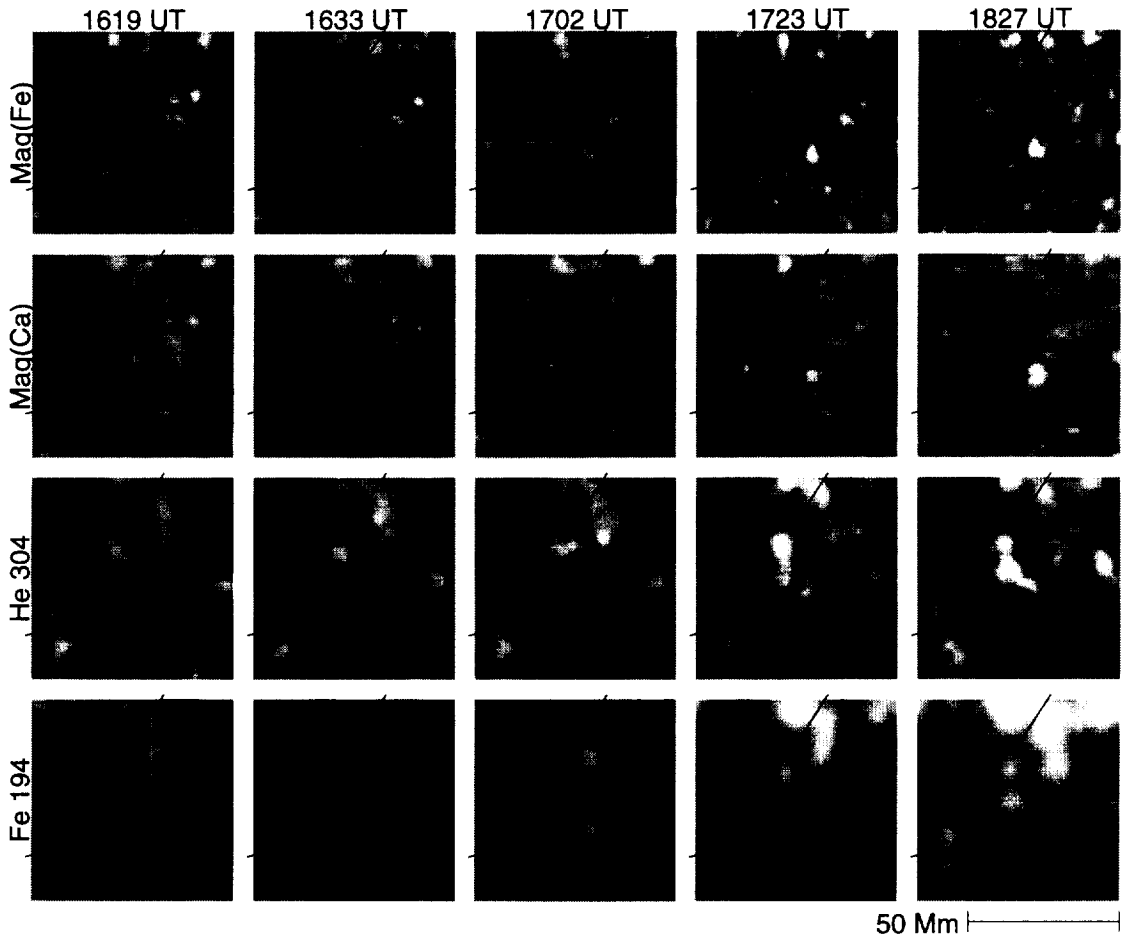

Figure 6. Section of the photospheric *Mag (Fe)* and chromospheric *Mag (Ca)* magnetograms of an emerging bipole *(at arrow)* observed on 16 June 1998. A second arrow points to an adjacent negative (black) polarity network element. The bottom two sets of panels show the corresponding EIT images in He II 304 Å and Fe XII 195 Å. The times of each vertical column of images is indicated at the top.

The 16 June 1998 data also had the largest of the emerging bipoles identified in our data. In this event, shown in images in Figure 6 and graphically in Figure 7, the bipole was detected in both the chromosphere and photosphere at essentially the same time, although a polynomial fit to the time variation of magnetic flux, in particular the positive polarity pole of the emerging region, suggests a delay of 10 to 25 minutes. This delay is similar to previous results (e.g. Harvey and Martin, 1973, *Solar Phys.*, **32**, 389). The He II 304 Å enhancement

associated with the emerging bipole is is first detected between 1822 and 1837 UT, similar to the deduced time of emergence of the magnetic fields in the chromosphere (1821–1835 UT). The associated coronal emission was faint and first observed at 1835 UT. By 2051 UT, the positive pole of the emerging bipole shows a loop connecting it to a negative network element about 32000 km to the southeast.

For the 14 emerging bipoles, we find that only 4 show any time delay between the photosphere and chromosphere; this delay is 15 to 35 minutes. However, 10 (71%) of the emerging bipoles appeared in the photospheric and chromospheric magnetograms at essentially the same time.

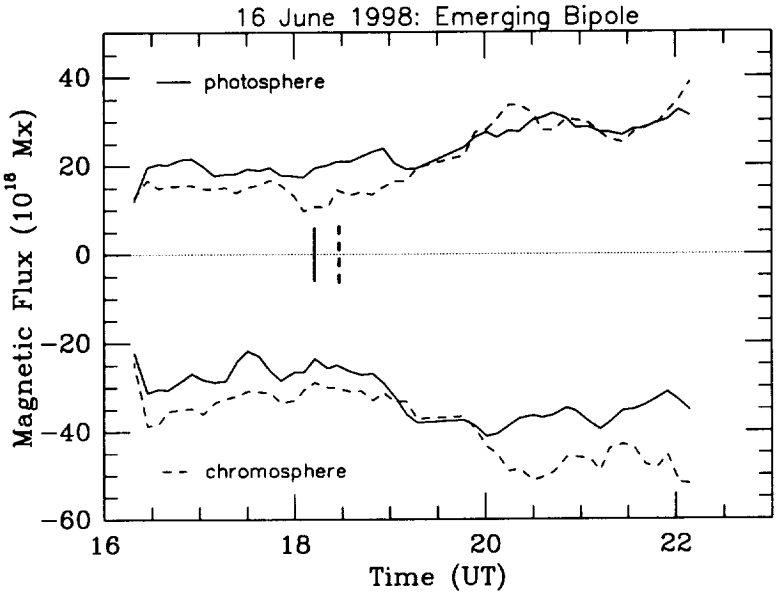

Figure 7. Plot of the positive and negative flux in the emerging bipole shown in the previous Figure. The vertical bars indicate the respective times of appearance of the region in the photosphere and chromosphere based on a polynomical fit to the data.

An interesting and unique aspect of the magnetic field data collected during the three observing campaigns is that we can directly compare the spatial distribution of individual magnetic structures observed in the photosphere and chromosphere. While we have done this for bipoles that are canceling and emerging, the more static, i.e. more slowly evolving, structures also show some curious differences. One example, involves two widely separated (36000 km) opposite magnetic network elements. The chromospheric magnetogram shows more diffuse magnetic structures than in the photosphere, a typical difference in the appearance of the magnetic flux elements betwene these two levels of the atmosphere. In this example, however, the diffuse chromsopheric fields are not symmetric about the underlying photospheric magnetic elements, but rather show a canopy that is more extended in one direction. This direction is closely aligned with the overlying coronal field as inferred from the corresponding Fe XII 195 Å image that shows a loop connecting the two oppositve polarity elements, bifrucaing at the east end to split between two separate, but adjacent positive magnetic elements. In a few instances, we have also noted displacements of the

magnetic network elements in the photosphere and chromosphere of 2-4 pixels (3300-6700 km) suggesting that some of the fields are non-radial. It is our intent to investigate these displacements, along with the non-symmetric canopies, in relation to the overlying coronal emmision structures and their implied magnetic field configuration.

2.2.2. Trace and MDI Observations

We are investigating two extended data sets of images taken by TRACE and SOHO/MDI beginning on 4 May 1998 and on 14 June 1998. As part ot this process, four-panel montages are being constructed from three TRACE images – Lyα 1215 Å, FeIX/X 171Å, and FeXII 195Å, and the corresponding high-resolution MDI magnetograms. These time-sequence data cover a 72-hour period with a cadence of 2.5 minutes. Examples of the 4-panel time sequence images of the combined MDI and TRACE observations are shown in Figures 8–10. Figure 8 shows the observations at roughly 3 hour intervals for an overall view of changes in the magnetic field, the chromosphere and corona during a 12-hour interval from 0100–1300 UT on 4 May 1998. Over the 12 hours, the large-scale pattern of magnetic flux remains about the same; in detail, however, magnetic flux elements have moved, disappeared, or new flux has emerged within the entire area observed. In total, 17 new ephemeral regions emerged within the field-of-view during the 12 hours of observation; this frequency translates to a bipole emergence rate of 0.6 ephemeral regions/10^{10} km^2 · hr, consistent with the previous observations. Each of the 17 emerging regions resulted in some enhancement of overlying coronal emission, although in most cases the emission was considered relatively minor.

Figure 9 shows an example of the emergence of a large ephemeral region and the associated atmospheric response to this emergence. For this emerging bipole, we find that Ly-α brightens within 15–20 minutes after the first detection of photospheric magnetic fields in the region. This is consistent with the timing inferred for the emerging bipole discussed above. The sites of the enhanced Ly-α signatures correspond to the magnetic poles of the region. It is almost an hour later that the coronal lines show increased emission. This emission is in the form of loops connecting the opposite polarity poles of the region. It also appears, as with larger emerging active regions, that both bright and dark expanding loops occur during the rapid emergence of magnetic flux. There also appear to be some transient changes in the surrounding faint coronal structures related to the emergence of magnetic flux. These changes, not shown in Figure 9, constitute a decrease in emission over an extended area surrounding the bipole, perhaps three times larger in dimension than the bipole. This decrease is followed by a re-establishment of faint coronal emission.

Figure 10 shows the chromospheric and coronal response to the cancellation or disappearance of a magnetic bipole. In this example, there are two poles of white or positive polarity converging on an opposite polarity network element. Before these magnetic structures come in contact with each other, connections form between the opposite polarity elements, appearing as generally unresolved coronal emission, but in some cases loops. The coronal and chromospheric emission is variable, with several rapid brightenings occurring associated in one instance with ejecta. The coronal emission associated with this cancelling feature is not longer evident more than one hour *before* the converging positive polarity structure completely disappears.

2.3. *SUMMARY*

Using collaborative observations of the photospheric and chromospheric magnetic fields,

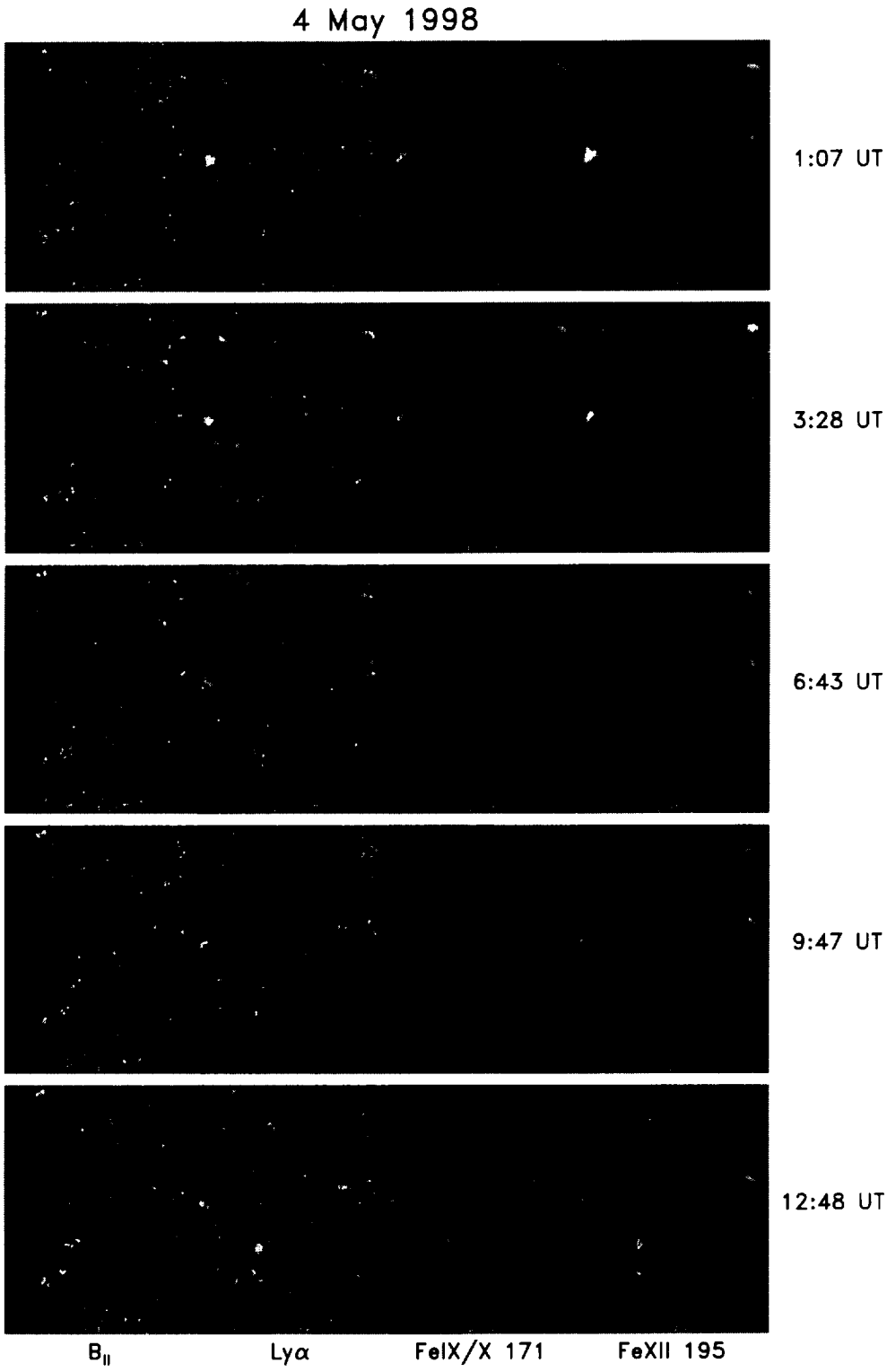

Figure 8. Selection of frames from 12 hour sequence of MDI magnetograms and TRACE images on 4 May 1998. The vertical dimension of the frames is 242 arcseconds.

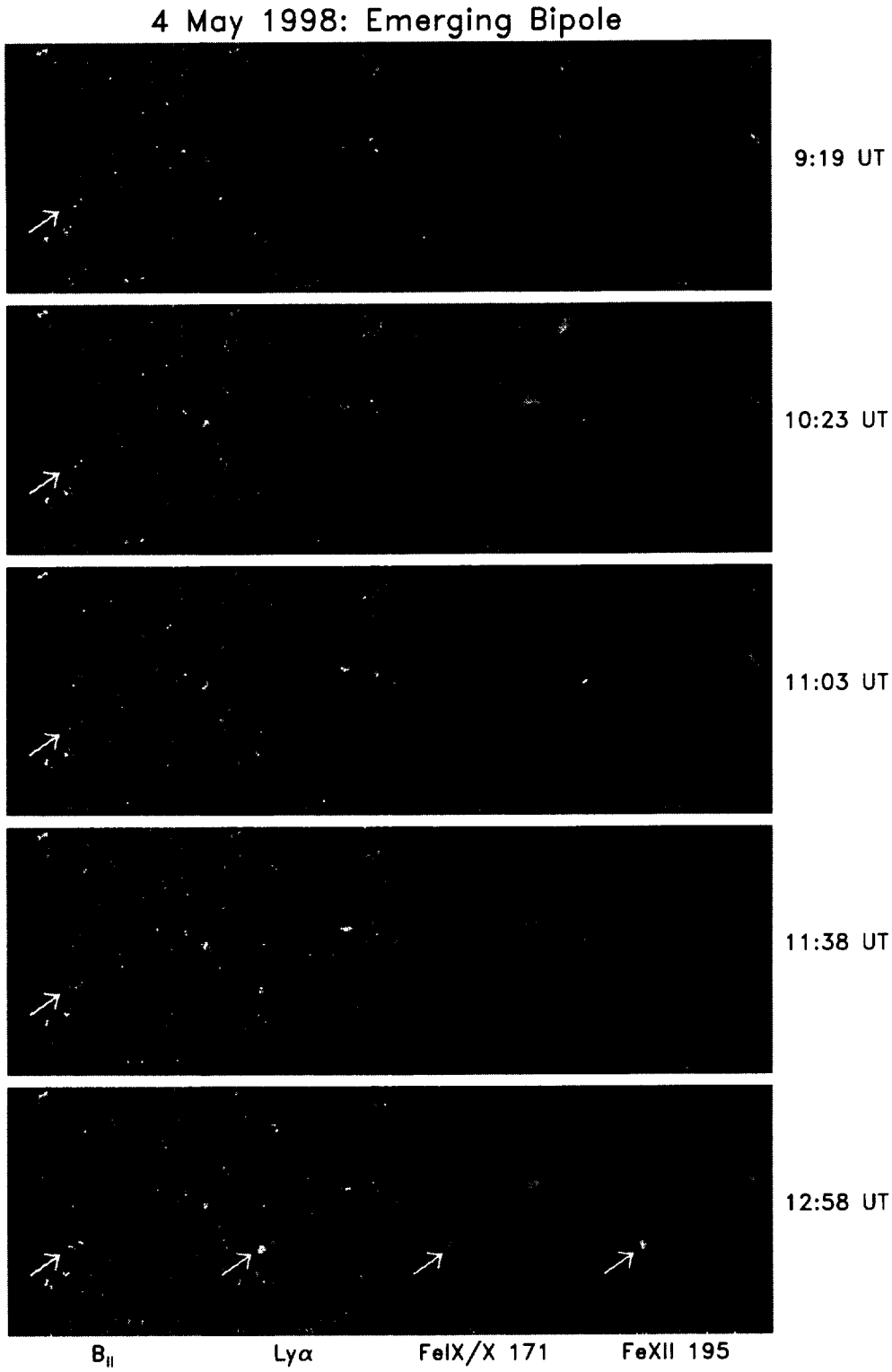

Figure 9. Selection of frames on 4 May 1998 showing the emergence of a magnetic bipole indicated by the *white arrows*. Note the coronal and chromospheric signature of this emerging region.

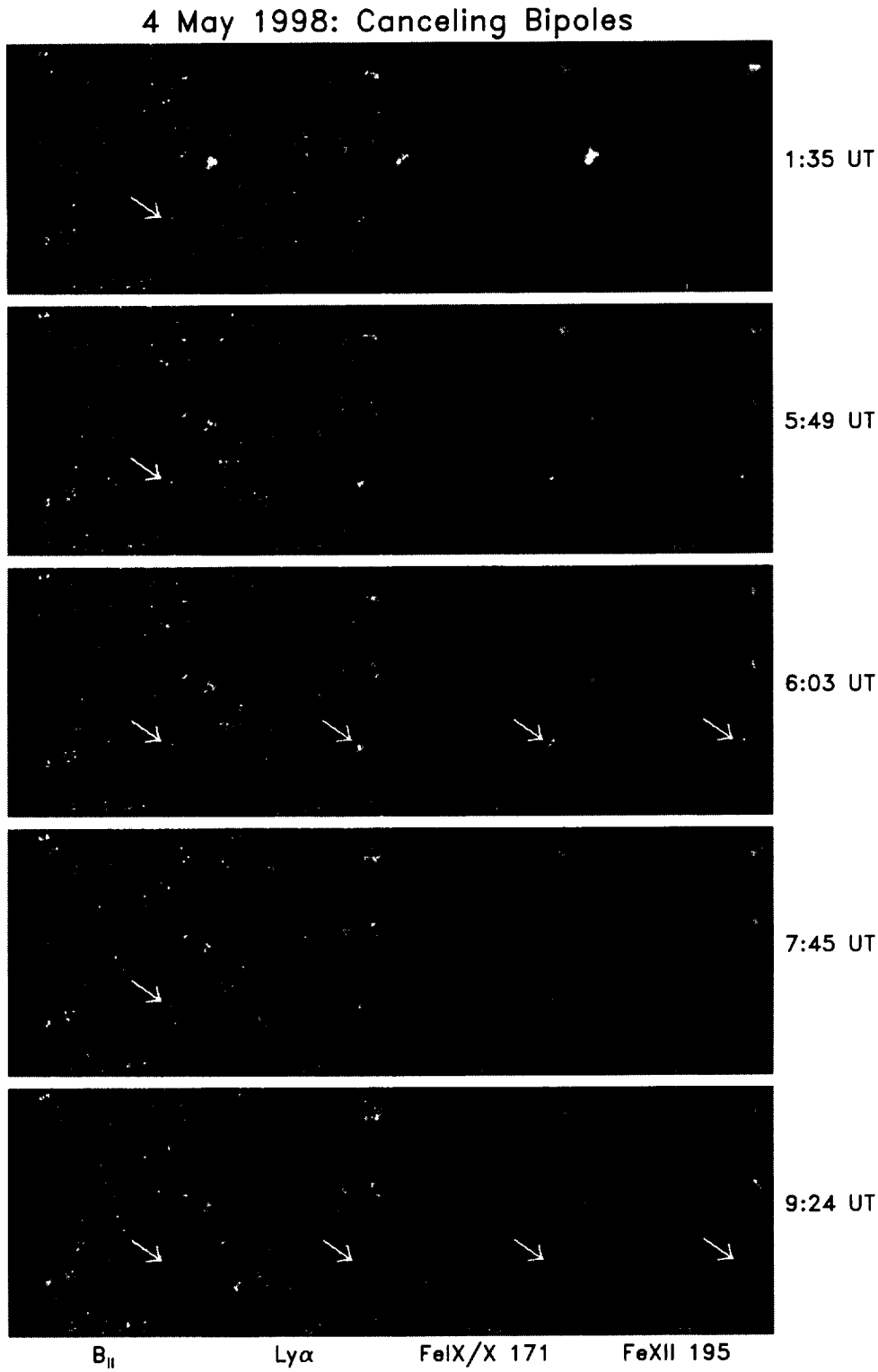

Figure 10. Selection of frames on 4 May 1998 showing the cancellation of a magnetic bipole indicated by the *white arrows*. Note the coronal and chromospheric signature of this canceling region.

along with intensity images from EIT and TRACE, we find that

- in 45 canceling bipoles, the magnetic flux disappears in the chromosphere before the photosphere (44%), at the same time (36%), and in the photosphere first (20%). This trend suggests that magnetic flux in slightly less than half of the canceling bipoles is submerging.
- for the events studied, the delay between the earlier flux disappearance in the chromosphere is consistent the timing of the disappearance of the coronal and chromospheric structures observed in the EIT images.
- in some emerging bipoles, there appears to be some delay in the emergence of a magnetic bipole in the photosphere and chromosphere, a result also suggested by the relative timing of the enhancement of the chromospheric and coronal emission structures. This is consistent with many previous results on the aspect of the evolution of magnetic flux emergence.

2.4. *FUTURE PLANS*

We are preparing three papers on the results of this analysis:

1. 'Does Magnetic Flux Submerge in Canceling Magnetic Bipoles?'
2. 'The Comparison of the Chromospheric and Photospheric Magnetic Fields, Their Height and Spatial Distribution'
3. 'The Evolution of the Chromospheric and Photospheric Magnetic Fields in Relation to EIT, TRACE, and SXT Observations'

to be co-authored by K. L. Harvey, H. Jones, M. Penn, and D. Hassler.

This will require complete the comparison of the magnetic field evolution with the EIT, TRACE, and SXT images to refine the timing of the height evolution of the evolving magnetic bipoles and to compare the timing of magnetic flux disappearnace and appearance with the MDI and BBSO magnetogtams.

REPORT DOCUMENTATION PAGE

Form Approved
OMB No. 0704-0188

1. AGENCY USE ONLY *(Leave blank)*	2. REPORT DATE	3. REPORT TYPE AND DATES COVERED
	1 August 1999	Final, 2 December 1997 – 1 August 1999

4. TITLE AND SUBTITLE
1. Helioseismic Holography
2. A Study of the Process of Magnetic Flux Disappearance in Canceling Bipoles

5. FUNDING NUMBERS
C: NASW-97029

6. AUTHORS
Karen L. Harvey and Charles Lindsey

7. PERFORMING ORGANIZATION NAME(S) AND ADDRESS(ES)
Solar Physics Research Corporation
4720 Calle Desecada
Tucson, AZ 85718

8. PERFORMING ORGANIZATION REPORT NUMBER
nasa-97029.f7

9. SPONSORING/MONITORING AGENCY NAME(S) AND ADDRESS(ES)
National Aeronautics and Space Administration
NASA Headquarters
Washington, DC 20546

10. SPONSORING/MONITORING AGENCY REPORT NUMBER

11. SUPPLEMENTARY NOTES

12a. DISTRIBUTION/AVAILABILITY STATEMENT
UNLIMITED

12b. DISTRIBUTION CODE

13. ABSTRACT *(Maximum 200 words)*

Project 1: We have developed and applied the technique of helioseismic holography along the lines originally set out in our proposal. The result of the application of this diagnostic technique to solar activity and the quiet Sun has produced a number of important discoveries: (1) acoustic moats surrounding sunspots, (2) acoustic glories surrounding large active regions, (3) acoustic condensations beneath active regions, (4) temporally-resolved acoustic images of a solar flare. These results have been published in a series of papers in the Astrophysical Journal. We think that helioseismic holography is now established as the most powerful and discriminating diagnostic in local helioseismology.

Project 2: We conducted a collaborative observational program to define the physical character and magnetic geometry of canceling magnetic bipoles aimed at determining if the cancellation process is the result of submergence of magnetic fields. This assessment is based on ground-based observations combining photospheric and chromospheric magnetograms from NSO/KP, BBSO, and SOHO-MDI, and EUV and X-ray images from SOHO EIT/CDS, Yohkoh/SXT, and TRACE. Our study involves the analysis of data taken during 3 observing campaigns, Sept 1997, May 1998, June 1998, to define the height structure of canceling bipoles inferred from magnetic field and intensity images, and how this varies with time. We find that some canceling bipoles can be explained by the submerge of their magnetic flux. A paper on the results of this analysis will be presented at a upcoming scientific meeting and be written up for publication.

14. SUBJECT TERMS	15. NUMBER OF PAGES
Helioseismology, Sunspots, Magnetic Fields	16. PRICE CODE

17. SECURITY CLASSIFICATION OF REPORT	18. SECURITY CLASSIFICATION OF THIS PAGE	19. SECURITY CLASSIFICATION OF ABSTRACT	20. LIMITATION OF ABSTRACT
UNCLASSFIED	UNCLASSIFIED	UNCLASSIFIED	